# Ising-Bloch transition for spatially extended patterns

Kestutis Staliunas
*ICREA, Departament de Fisica i Enginyeria Nuclear, Universitat Politècnica de Catalunya, Colom, 11, E-08222 Terrassa, Barcelona, Spain*

Víctor J. Sánchez-Morcillo
*Departament de Fisica Aplicada, Escuela Politécnica Superior de Gandia, Universidad Politécnica de Valencia, Ctra. Natzaret-Oliva S/N, 46730-Grao de Gandia, Spain*

(Received 30 July 2004; published 8 July 2005)

The Ising-Bloch transition for domain walls in spatially extended nonlinear systems is a known phenomenon. We show a similar transition for extended patterns, such as labyrinths and stripes. The analysis is performed in the frame of the parametrically driven Ginzburg-Landau equation, which is a paradigmatic model for a variety on nonlinear systems showing the Ising-Bloch transition of domain walls.

DOI: 10.1103/PhysRevE.72.016203 PACS number(s): 05.45.−a, 47.54.+r, 42.65.−k

## I. INTRODUCTION

The parametrically driven Ginzburg-Landau equation (PGLE) for the complex-valued order parameter $A(r,t)$

$$\frac{\partial A}{\partial t} = (\mu + i\nu)A + \gamma A^* + d\nabla^2 A - (1+ic)|A|^2 A, \qquad (1)$$

is a generic model describing the slow phase and amplitude modulations of a spatially distributed assembly of coupled oscillators in simultaneous presence of Hopf and saddle-node bifurcations. It is perhaps the simplest model describing phase domains, and the Ising and Bloch walls between the phase domains, in spatially extended systems [1]. It finds applications in a large variety of nonlinear physical systems, such as parametrically driven chains of coupled pendula [2], or surface waves in deep liquid channels [3] and granular layers [4]. Of special interest is the relation of Eq. (1) with nonlinear optics, since the PGLE is an order parameter equation for different nonlinear optical resonators, such as degenerate optical parametric oscillators [5], four wave mixing in driven resonators [6], and resonators with Kerr-nonlinearity accounting for two polarization components of the fields [7].

In Eq. (1) the parameter $\mu$ measures the distance from the Hopf bifurcation point, and represents the coefficient of coherent (phase invariant) gain, if positive, or the coefficient of losses, if negative. In nonlinear optical resonators it corresponds to the net coherent amplification of the light (the gain minus loss). The parameter $\gamma$ corresponds to the forcing amplitude with a frequency twice that of the Hopf bifurcation, and measures the distance to the saddle-node bifurcation point. In degenerate nonlinear optical systems, where parametric generation or four wave mixing takes place, it corresponds to a parametric (phase squeezed) gain. The parameter $\nu$ represents the off-resonance detuning, which in nonlinear optical systems denotes the difference between the frequency of the forcing amplitude and that of the closest resonance mode of the resonator. The coefficient of the Laplace operator $d=d_{re}+id_{im}$ is the diffusion/diffraction coefficient, and is complex in general. In nonlinear optics typically diffraction prevails against diffusion, and the relation $d_{\mathrm{Im}} \gg d_{\mathrm{Re}}$ holds.

The coefficient of nonlinearity in nonlinear optical systems is usually real, or nearly real, ($|c| \ll 1$), which means that the saturation of the generated waves is the main source of the nonlinearity. However, in some cases the real and imaginary parts of the nonlinearity coefficient are of the same order of magnitude, e.g., for resonators with Kerr media with focusing/defocusing effects, for semiconductor resonators, where nonlinear focusing-defocusing occurs due to the so called $\alpha$ factor, or for optical parametric oscillators with pump detuning.

At high forcing amplitudes, when $\gamma \gg \mu$, Eq. (1) leads to perfectly phase squeezed patterns with real-valued order parameters. The nature of these patterns depends on the value of detuning. For small detuning ($\nu \ll \gamma$) Eq. (1) supports phase domains, for large detuning ($\nu \gg \gamma$) supports stripes, while for intermediate detuning supports patterns in the form of labyrinths [8], phase solitons [9], and hexagons [10], in the limit $\gamma \gg \mu$.

In the opposite limit $\mu \gg \gamma$ (or equivalently when the Hopf bifurcation point is closer than the saddle-node bifurcation point in the parameter space), the vortices [11] as localized structures, and tilted waves [12] or crossroll patterns [13] as extended patterns, can be expected. For intermediate values of the parameters the transition between these two phase-squeezed and phase-invariant patterns occurs. For the particular case of phase domains this transition is known as the Ising-Bloch transition [1]. The main result of the present paper is the prediction of a similar transition for extended patterns, and the investigation of its properties. The Ising-Bloch transition for extended patterns described in this paper has not been reported previously in the literature, and could find applications in a variety of nonlinear systems, those described by Eq. (1).

In Sec. II we overview the domain wall dynamics at small detuning, i.e., we discuss the Ising-Bloch transition of domain walls. There is a large activity on studies about the Ising-Bloch transition (see, e.g., Ref. [14], where the stability of domain walls in presence of modulational instabilities leading to labyrinthic patterns is considered). We generalize the existing results to the nonvariational cases of Eq. (1).

 

Next, in Sec. III we generalize the Ising-Bloch transition to extended patterns (stripes and labyrinths) appearing at intermediate and large values of detuning. Finally, in Sec. IV we conclude and shortly discuss the possible generalization of the Ising-Bloch transition to two-dimensional patterns, such as hexagons and phase (dark-ring) solitons.

## II. DOMAIN WALLS IN THE PDGLE

Domain walls are localized structures connecting two different solutions in different regions of space. For Eq. (1), the stationary and spatially homogeneous solution is given by the complex amplitude $A=|a|\exp(i\varphi)$, where

$$|a|^2=\frac{\mu+\nu c+\sqrt{(1+c^2)\gamma^2-(\nu-\mu c)^2}}{1+c^2}, \tag{2a}$$

$$\tan(2\varphi)=\frac{c|a|^2-\nu}{|a|^2-\mu}. \tag{2b}$$

The linear stability analysis shows that the homogeneous solution (2a) and (2b) is stable against pattern forming instabilities for small detunings. In the purely diffractive case $d_{re}=0$, corresponding, e.g., to optical systems, this stability condition is given by $\nu<c(\gamma+\mu)$.

The solution given by Eq. (2a) and (2b) implies the existence of two nonzero homogeneous states with the same intensity value and amplitudes with opposite sign or, in terms of phase, related by $\varphi_2=\varphi_1+\pi$. Owing to this symmetry, the fields are perfectly phase squeezed. These two solutions, when realized in different spatial regions, constitute phase domains, and the lines separating these two solutions the domain walls. The domain walls are stable in the case of small detuning, in accordance with the stability properties of the homogeneous background solutions.

Equation (1) admits two analytical solutions in the form of domain walls, namely Ising and Bloch walls. For the Ising wall, the phase jumps abruptly from $-\pi$ to $+\pi$ across the boundary, whereas for Bloch walls the phase changes smoothly. As a consequence, the amplitude of the order parameter at the core of the wall vanishes for Ising walls, but not for Bloch walls. For this reason, Ising and Bloch walls are sometimes referred as black and grey walls. In the nonvariational cases, there are also dynamical differences: Bloch walls are nonstationary and drift at a constant velocity, the motion resulting from the breaking of the chiral symmetry.

The amplitude distribution of a straight [one-dimensional (1D)] Ising domain can be found analytically in the form

$$A_I(x)=A\tanh(x/x_0), \tag{3}$$

where $A$ is the homogeneous solution of Eq. (1) and $x_0$ is the width of the domain wall given by

$$x_0^2=\frac{2d}{(1+ic)|a|^2}. \tag{4}$$

The Ising domain boundary solution has been previously obtained in the variational limit of Eq. (1), corresponding to $\nu=c=d_{im}=0$ [1]. We note, however, that the solution in the form of Eq. (4) is valid also in the nonvariational case, resulting in a domain wall in form of an hyperbolic tangent of complex argument. This results in periodically oscillating fronts of domain boundary, as illustrated in Fig. 1(a).

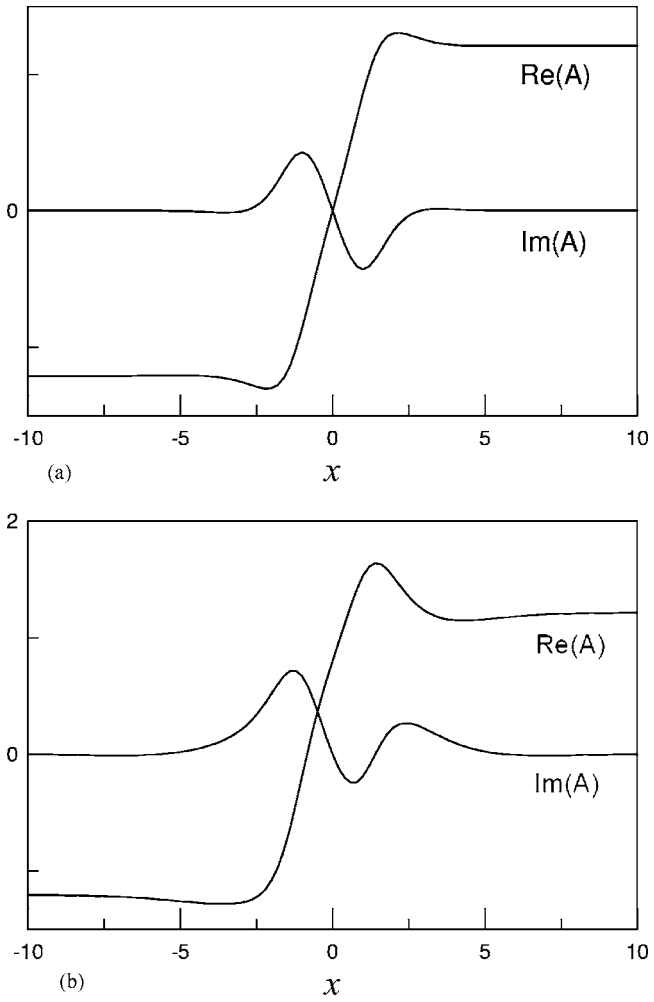


FIG. 1. Spatial distribution of Ising (a) and Bloch (b) walls, obtained from the analytical solutions given by Eqs. (3)–(5). Parameters are $c=0.2$, $\nu=0.1$, $\gamma=0.5$, $\mu=1$, $d_{\mathrm{Re}}=0$, and $d_{\mathrm{Im}}=1$. For the Bloch wall, the amplitude $B=0.8$ has been chosen arbitrarily, which, however, corresponds to a particular point in parameter space.

When the distances to the Hopf and saddle-node bifurcation points are of the same order, $\gamma\approx\mu$, the phase of resulting patterns might be only partially squeezed. The domain boundary is then of Bloch type, and obeys the analytical form

$$A_B(x)=A\tanh(x/x_0)\pm iB\,\mathrm{sec}\,h(x/x_0), \tag{5}$$

where the signs of the second term correspond to the two possible chiralities of the wall. The solution (5) exists in variational as well as in the nonvariational case, where in the latter case the width of the domain boundary $x_0$ is complex. The amplitude $A$ corresponds again to the homogeneous background solution. The amplitude $B$ in variational case is given by simple expression $B=\sqrt{\mu-3\gamma}$; however, no simple

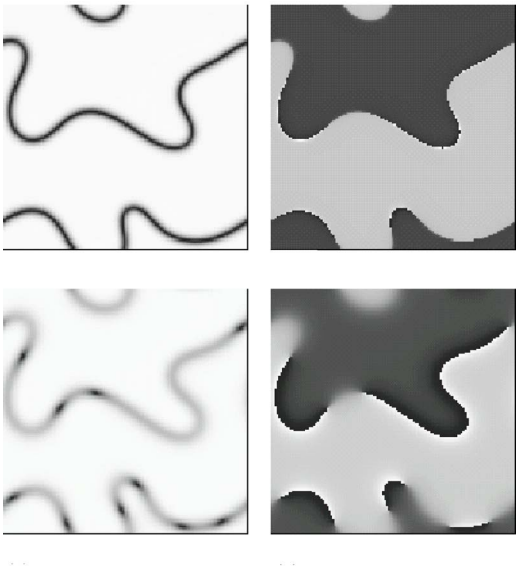

FIG. 2. Ising (top row), and Bloch (bottom row) domain walls, as found by numerical integration of Eq. (1) in two spatial dimensions. The intensity (left) and phase (right) patterns are depicted. Periodic boundary conditions (here and in other calculations throughout the article) were used on a spatial domain of unit size. The parameters used: $\nu=0.1$, $\mu=2$, $d_{\mathrm{Re}}=0.0005$, $d_{\mathrm{Im}}=0.0001$, and $c=0$. The forcing amplitude for Ising domains is $\gamma=1$, and for Bloch domains $\gamma=0.3$. The two-dimensional calculations in were performed on the grid of (128X128).

analytic expression exist in the nonvariational case. In Fig. 1(b) the amplitude distribution of a Bloch wall is shown as given by Eq. (5) for arbitrarily chosen parameters $A,B$, and $x_0$. We note that since in nonsingular regions there exist a nonsingular mapping between the parameters of the PGLE (1) and the parameters of the Bloch wall (5), the arbitrarily chosen parameters corresponds to a particular point in parameter space of PGLE.

The transition between Ising and Bloch walls in the variational case $\nu=c=d_{im}=0$ occurs at $\gamma=\mu/3$ [1]. For $\gamma$ larger (smaller) than this critical value, the domain boundaries are of Ising (Bloch) type. In the nonvariational case the transition point can be found analytically by matching the solutions (4) and (5), but again does not leads to analytically tractable results.

In two spatial dimensions the situation is more complex. Figure 2 shows two examples of the intensity distribution in presence of Ising and Bloch domain walls, where the nearly variational limit ($d_{\mathrm{Im}} \ll d_{\mathrm{Re}}$, $\nu \ll 1$) has been considered. The most characteristic feature for the two-dimensional (2D) Bloch domain walls is that they typically contain elliptically shaped (phase-squeezed) vortices: the domain boundary surrounding a phase domain resembles a necklace of vortices. In other words, a Bloch domain wall, like shown in Fig. 2(b), consists of pieces of Bloch walls of different chiralities, separated by vortices. This occurs, for example, if during the Ising-Bloch transition the chirality along the domain wall acquires random values due, e.g., to a spatially random seed. Similar vortex chain patterns have been reported in Ref. [15] for a type-II optical parametric oscillator.

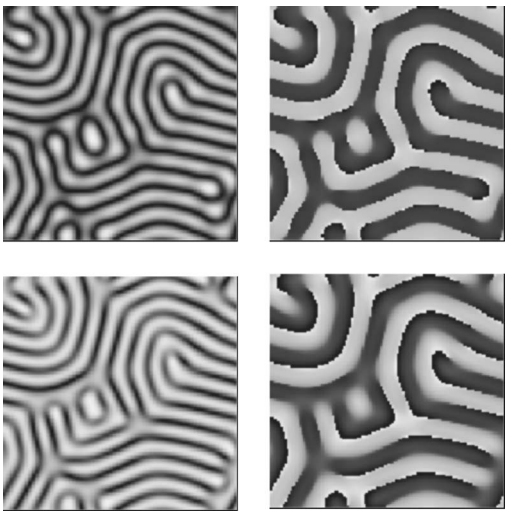

FIG. 3. Ising-like (top row), and Bloch-like (bottom row) labyrinths. Everything as in Fig. 2, except for $\nu=1$, $\gamma=0.7$. Values of $\mu$ are $\mu=0$ for Ising domains, and $\mu=1.5$ for Bloch domains.

## III. ISING-BLOCH TRANSITION OF LABYRINTS AND STRIPES

The main purpose of the article is to identify and describe the Ising-Bloch transition for extended patterns, on the basis of analogies with the above described corresponding transition for (localized) domain walls. The extended patterns, as mentioned above, appear for large $\nu \gg \gamma$ detunings (in the form of 1D striped patterns), but also for moderate $\nu \approx \gamma$ detunings (in the form of 2D hexagons and labyrinths). This happens in particular in the optical limit of Eq. (1), characterized by $d_{\mathrm{Im}} \gg d_{\mathrm{Re}}$. Figure 3 shows a labyrinth pattern obtained by numerical integration of Eq. (1) for moderate detuning. Similar patterns have been reported in Ref. [16]. The situation depicted in Fig. 3 is similar to that shown in Fig. 2. The dark lines in labyrinths are at some places (typically at the edges) grey, remaining at other places dark. Also the chirality sometimes change the sign along a grey line in such labyrinths. All this indicates a similarity between Ising-Bloch transition for domain walls and for extended patterns, and we refer to these patterns as Bloch-like labyrinths, in contrast to Ising-like labyrinths where the grey lines and vortices are absent.

We perform the analytical study of the Ising-Bloch transition for extended patterns, considering the simplest 1D pattern in the form of stripes, described by

$$A(x,t) = a_+(t)\exp(ikx + i\omega t) + a_-(t)\exp(-ikx - i\omega t) + (\text{higher-order terms}), \tag{6}$$

where the moduli $a_\pm$ of the constituent tilted waves are not necessarily equal one to another. In the following we consider near-resonant stripes, for which the dispersion relation $dk^2 - \nu \equiv \Delta\nu$, with $|\Delta\nu| \ll \nu$, holds. Also we consider the "optical" limit of the Eq. (1), taking for simplicity $c=d_{re}=0$. Inserting the ansatz (6) into Eq. (1), neglecting terms oscillating at third and higher spatial harmonics, and assuming

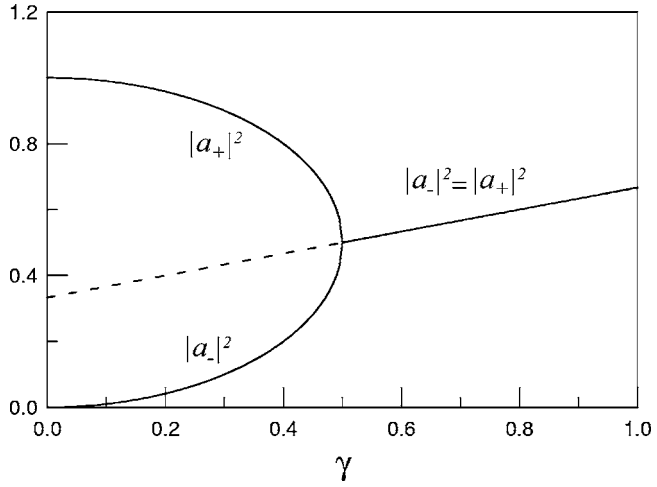


FIG. 4. The amplitudes of the tilted waves for symmetric Ising and for asymmetric Bloch solution, as given by (8) and (9) with $\mu=1$.

stationary solutions one obtains the following amplitude equations

$$i\omega a_+ = (\mu - |a_+|^2 - 2|a_-|^2)a_+ + \gamma a_-^* - i\Delta\nu a_+, \quad (7a)$$

$$-i\omega a_- = (\mu - 2|a_+|^2 - |a_-|^2)a_- + \gamma a_+^* - i\Delta\nu a_-. \quad (7b)$$

The Ising-like stripe pattern corresponds to the symmetric solution of Eqs. (7a) and (7b), given by

$$|a_+|^2 = |a_-|^2 = \frac{\mu + \sqrt{\gamma^2 - \Delta\nu^2}}{3}, \quad (8)$$

with $\omega=0$, which is stable for $\gamma \gg \mu$. The spatially harmonic stripe solution (8) is, strictly speaking, valid for $\mu, \gamma \ll 1$, in order to ensure the smallness condition for the higher order harmonics.

The stability analysis shows that the symmetric Ising stripe (8) becomes unstable for $\gamma < \mu/2$. Instead, the asymmetric solution $|a_+| \neq |a_-|$ sets in, which corresponds to Bloch-like stripes. An analytical expression of the asymmetric solution of Eqs. (7a) and (7b) is complicated in general. Restricting, however, to the resonant case $\Delta\nu=0$, one finds the solution

$$|a_\pm|^2 = (\mu \pm \sqrt{\mu^2 - 4\gamma^2})/2, \quad (9)$$

for $\omega=0$. The two signs in (9) correspond to the two possible chiralities of the Bloch stripes.

The solutions (8) and (9) are plotted in Fig. 4. The transition between Ising and Bloch stripes in this case occurs at a critical point $\gamma/\mu = 1/2$.

The numerical integration of Eq. (1) shows the above predicted Ising-Bloch transition of stripes. Bloch-like stripe patterns are characterized by a nonzero value of its minimal amplitude (corresponding to grey intensity patterns). In Fig. 5 the maximal and minimal values of the stripe patterns have been numerically evaluated as a function of the forcing amplitude $\gamma$. The numerical results confirm the analytically predicted value of $\gamma/\mu = 1/2$ for the Ising-Bloch transition of

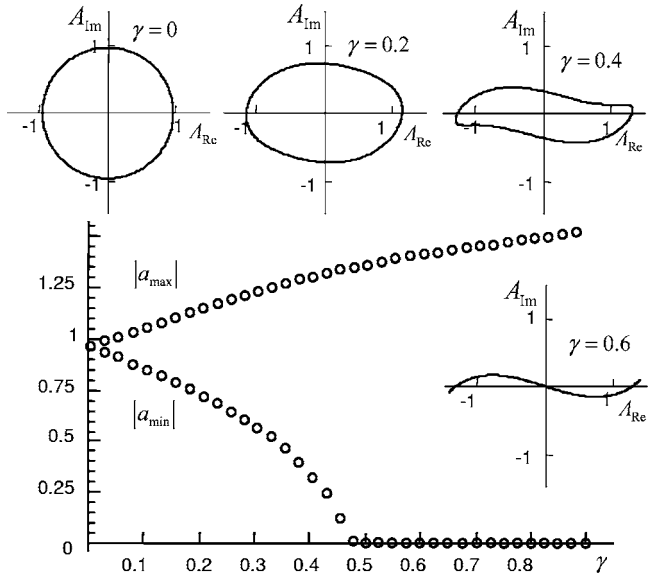


FIG. 5. Maximal and minimal amplitude of the field in the stripe pattern depending on the forcing amplitude $\gamma$ for the resonant stripes, as obtained by numerical integration of Eq. (1). Insets show the phase portraits of the Ising and Bloch walls. The parameters used: $\nu=0.64$, $\mu=1$, $d_{\rm Re}=0.0001$, $d_{\rm Im}=0.001$, and $c=0$. The wave number of the stripe is $|k|=4\cdot 2\pi$. The one-dimensional calculations in were performed on the grid of 2048 points.

stripes close to the threshold, and leads to slightly different values far away from the threshold, when the third harmonics are no more negligible. The insets in Fig. 5 shows numerically obtained phase portraits of Ising and Bloch stripes at selected values of $\gamma$.

The Ising-Bloch transition can be alternatively interpreted as a symmetry-breaking bifurcation of the chirality parameter, defined as the imaginary part of the order parameter at the core of the wall [1], $\chi = \mathrm{Im}\, A(0)$. The minimal amplitude

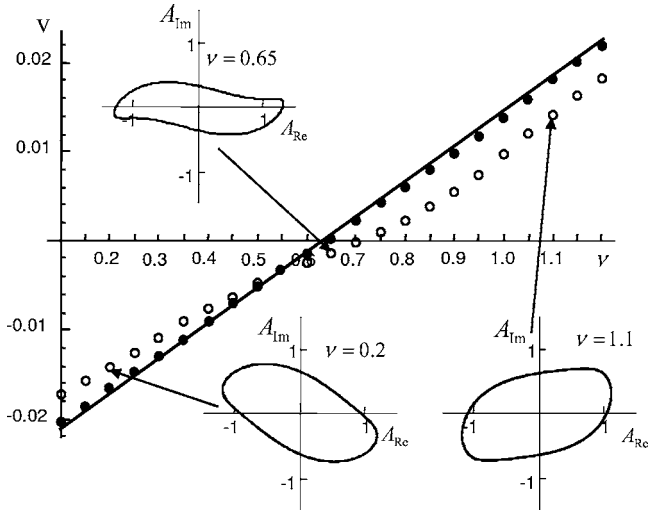


FIG. 6. Velocity of the stripe pattern depending on the detuning as obtained by numerical integration of Eq. (1) for two values of $\gamma=0.4$ (black symbols) and 0.2 (white symbols). The straight line is the analytical dependence for the perfect tilted wave at $\gamma=0$. The parameters are as in Fig. 5.

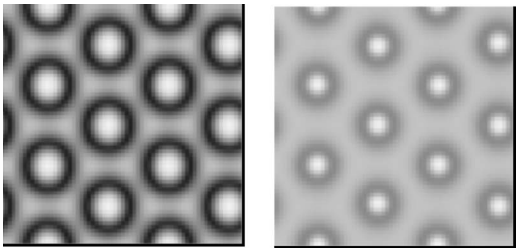

FIG. 7. Ising and Bloch-like hexagons as obtained by numerical integration of Eq. (1) with the parameters $\nu=0.5$, $\gamma=0.5$. $d_{\mathrm{Re}}=0.0001$, $d_{\mathrm{Im}}=0.001$, and $c=0$, for two different values of $\mu=0$ and 1.2.

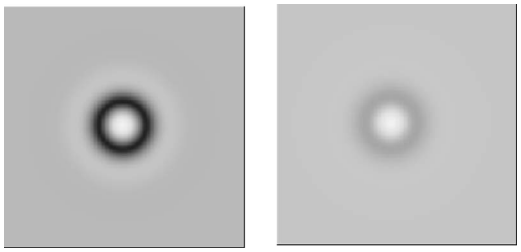

FIG. 8. Ising and Bloch-like dark ring spatial solitons as obtained by numerical integration of Eq. (1) with the parameters $\nu=0.4$, $\gamma=0.4$, $d_{\mathrm{Re}}=0.0001$, $d_{\mathrm{Im}}=0.0015$, and $c=0$, for two values of $\mu=0$ and 2.

of the field is proportional to chirality (a null chirality corresponds to symmetric, Ising patterns), and consequently Fig. 5 also represents the chirality as a function of $\gamma$.

The resonant Bloch stripes are stationary, since the resonant solutions (9) have zero oscillation frequency, $\omega=0$. The oscillation frequency of off-resonance stripes is, however, nonzero, $\omega\neq 0$, and therefore the off-resonant Bloch stripes move. An analytically tractable solution of Eqs. (7a) and (7b) is possible in limiting cases, e.g., in the limit $|a_+|\ll|a_-|$ when one tilted wave strongly dominates, and close to the resonance $|\Delta\nu|\ll 1$. This results in a simple asymptotic expression for the oscillation frequency $\omega=-\Delta\nu$, and correspondingly for the velocity of motion of Bloch stripes $v=\omega/k=-\Delta\nu/k$. Figure 6 shows the dependence of the velocity of stripes with detuning as calculated numerically, which are in a good agreement with the analytical result, especially in the limit of a strong domination of one tilted wave.

We note to the point that similar solutions were numerically found for laser with squeezed injection, and were named as imperfect tilted waves [17].

## IV. CONCLUSIONS

We have shown a transition between perfectly and partially phase-squeezed extended patterns, such as stripes and labyrinths. This transition is analogous to the Ising-Bloch transition of domain walls, and we identify it as the Ising-Bloch transition of extended patterns. The transition, reported here is analytically investigated by means of amplitude equations for one-dimensional stripe patterns in the parametrically driven Ginzburg-Landau equation, and numerically confirmed for stripes (one spatial dimension) and labyrinths (two spatial dimensions).

Our numerical investigation in the two-dimensional case allows us to identify a similar transition between grey-line and dark-line dominated pattern for hexagons and for the phase (dark-ring) spatial solitons. Numerical examples of the two kinds of patterns (Ising and Bloch like) are shown in Fig. 7 (for hexagons [10]) and Fig. 8 (for phase solitons [9]), where a transition between the dark-line and grey-line dominated patterns is observed. The extension of the ideas presented in this paper to these essentially two-dimensional patterns (hexagons and stripes) is in progress.

## ACKNOWLEDGMENTS

The work was financially supported by the CICYT of the Spanish Government, under the Project No. BFM2002-04369-C04-04. K.S. acknowledges support by Project No. FIS2004-02587 of the Spanish Ministry of Science and Technology. We gratefully acknowledge discussions with G.J. de Valcárcel and E. Roldán.

[1] P. Coullet, J. Lega, B. Houchmanzadeh, and J. Lajzerowicz, Phys. Rev. Lett. **65**, 1352 (1990)
[2] I. V. Barashenkov, S. Woodford, and E. V. Zemlyanaya, Phys. Rev. Lett. **90**, 054103 (2003).
[3] J. W. Miles, J. Fluid Mech. **148**, 451 (1984).
[4] L. S. Tsimring and I. S. Aranson, Phys. Rev. Lett. **79**, 213 (1997).
[5] S. Longhi, Opt. Lett. **20**, 695 (1995).
[6] V. B. Taranenko, K. Staliunas, and C. O. Weiss, Phys. Rev. Lett. **81** 2236 (1998).
[7] V. J. Sánchez-Morcillo, I. Pérez-Arjona, F. Silva, G. J. de Valcárcel, and E. Roldán, Opt. Lett. **25**, 957 (2000).
[8] A. Yochelis, A. Hagberg, E. Meron, A. L. Lin, and H. L. Swinney, SIAM J. Appl. Dyn. Syst. **2**, 236 (2002).
[9] K. Staliunas and V. J. Sanchez-Morcillo, Phys. Lett. A **241** 28 (1998).
[10] I. S. Aranson, L. S. Tsimring, and V. M. Vinokur, Phys. Rev. E **59**, R1327 (1999).
[11] P. Coullet, L. Gil, and F. Rocca, Opt. Commun. **73**, 403 (1989).
[12] Q. Feng, J. V. Moloney, and A. C. Newell, Phys. Rev. Lett. **71**, 1705 (1993).
[13] K. Staliunas and C. O. Weiss, Physica D **81**, 79 (1995).
[14] B. Marts, A. Hagberg, E. Meron and A. L. Lin, Phys. Rev. Lett. **93**, 108305 (2004).
[15] G. Izús, M. San Miguel, and M. Santagiustina, Phys. Rev. E **64**, 056231 (2001).
[16] G. J. de Valcárcel and K. Staliunas, Phys. Rev. E **67**, 026604 (2003).
[17] O. G. Calderón, E. Cabrera, M. A. Antón, I. Gonzalo, F. Carreño, and J. M. Guerra, Phys. Rev. Lett. **92**, 163901 (2004).